Electric Power Systems Research 212 (2022) 108555

Contents lists available at ScienceDirect

Electric Power Systems Research

journal homepage: www.elsevier.com/locate/epsr

Coordinated day-ahead dispatch of multiple power distribution grids hosting stochastic resources: An ADMM-based framework

Rahul Gupta *, Sherif Fahmy, Mario Paolone

Distributed Electrical Systems Laboratory, EPFL, Lausanne, Switzerland

ARTICLE INFO

Keywords:
Dispatching
Multi-grid dispatch
Distributed optimization
Stochastic optimization
ADMM

ABSTRACT

This work presents an optimization framework to aggregate the power and energy flexibilities in an interconnected power distribution systems. The aggregation framework is used to compute the day-ahead dispatch plans of multiple and interconnected distribution grids operating at different voltage levels. Specifically, the proposed framework optimizes the dispatch plan of an upstream medium voltage (MV) grid accounting for the flexibility offered by downstream low voltage (LV) grids and the knowledge of the uncertainties of the stochastic resources. The framework considers grid, i.e., operational limits on the nodal voltages, lines, and transformer capacity using a linearized grid model, and controllable resources' constraints. The dispatching problem is formulated as a stochastic-optimization scheme considering uncertainty on stochastic power generation and demands and the voltage imposed by the upstream grid. The problem is solved by a distributed optimization method relying on the Alternating Direction Method of Multipliers (ADMM) that splits the main problem into an aggregator problem (solved at the MV-grid level) and several local problems (solved at the MV-connected-controllable-resources and LV-grid levels). The use of distributed optimization enables a decentralized dispatch computation where the centralized aggregator is agnostic about the parameters/models of the participating resources and downstream grids. The framework is validated for interconnected CIGRE medium- and low-voltage networks hosting heterogeneous stochastic and controllable resources.

1. Introduction

The current power system faces significant operational challenges due to the accelerated deployment of intermittent distributed energy resources (DERs) (e.g., photovoltaic—PV, wind, small hydro, energy storage, and electric-vehicle-charging-stations). On the one hand, it increases the reserve requirements in the power transmission grids; while, on the other hand, it is the origin of operational issues in power distribution systems associated with the quality-of-service (voltage regulation) and lines/transformer congestions.

Conventionally, the power imbalances are handled by a centralized entity (*Balance Service Provider—BSP* - e.g., [1]) that is responsible for coordination between generation and consumption at all times. This entity buys contracts from large centralized units such as hydropower plants to provide balancing power in case of imbalances [1,2]. However, with the growing penetration of stochastic (e.g., PV) as well as controllable (e.g., energy storage) DERs, there is an opportunity to aggregate local resources' flexibility [3–8]. However, DERs are often characterized by small capacities, unlike "conventional" generating units, and therefore insufficient to meet the existing thresholds for participating to day-ahead balancing markets. Therefore, aggregation of flexibilities from multiple DERs would be interesting as proposed in [9,10]. Several such aggregation models are summarized in [11].

Several works have proposed to aggregate the flexibility of multiple micro-grids (MGs) (e.g., [12,13]). However, these works are only limited to low voltage (LV) systems. In [13], authors proposed multi-microgrid optimal dispatch algorithms where stochastic and probabilistic models of microgrids and energy resources are embedded into the day-ahead-dispatch-plan computation. The problem is solved using a heuristic-based algorithm, and does not include the operational constraints of the grid. In [14], a method to evaluate the flexibility of distribution grids that can be provided to the upstream system, is proposed. More specifically, the problem first quantifies the flexibility offered by different units within the downstream grid, and then aggregates the result of the first-phase to the upstream system. However, the computation is unidirectional and, therefore, does not consider other resources of flexibility. In [15], a cooperative dispatch scheme is proposed where the transmission network was divided into different areas where their respective dispatch-plans were computed by using a distributed optimization framework. Grid constraints are also ignored in this approach. Finally, the work in [16] solves a multi-level power

* Corresponding author.
E-mail addresses: rahul.gupta@epfl.ch (R. Gupta), sherif.fahmy@epfl.ch (S. Fahmy), mario.paolone@epfl.ch (M. Paolone).

https://doi.org/10.1016/j.epsr.2022.108555
Received 9 October 2021; Received in revised form 16 April 2022; Accepted 2 July 2022
Available online 3 August 2022

system dispatch problem where the grid constraints are modeled by leveraging the DC-approximation of the load-flow equations. However, as known, the DC-flow approximation of the power-flow equations does not yield accurate results for distribution grids since the grid branch impedances are characterized by high resistance to reactance ratio (i.e., R/X ≥ 1). In [17], a medium voltage feeder was dispatched with a controllable Battery Energy Storage System (BESS) but without accounting for downstream LV systems.

In this context, this paper proposes a grid-aware optimization framework capable to aggregate power and energy flexibility from downstream LV systems to the upstream MV system. The aggregation is used to achieve the dispatch of a MV network considering the flexibility of multiple downstream LV networks and controllable resources (e.g. BESSs). A direct consequence of the proposed formulation is also the determination of the aggregate dispatch-plans of the different MV-connected LV-downstream-grids. First, the coordination problem is formulated as a centralized optimization. However, such a approach may rapidly increase the number of decision variables for a large system comprising of several networks and controllable DERs. Also, the parameters of all networks are not publicly available and not shared. These issues are usually solved by distributed optimization schemes as in [18–25]. In this respect, we use an Alternating Direction Method of Multipliers (ADMM)-based distributed optimization scheme that guarantees an inter-grid-layer-privacy (here, the privacy concerns the networks' and DERs' models). It consists of a main aggregator and sub-problem-solvers. The aggregator is the MV network DSO, whereas the sub-problem-solvers are MV-connected controllable entities such as resources (e.g. BESS) and downstream LV systems. The aggregator solves an optimal power flow (OPF) considering the uncertainty of both the upper-layer-transmission-grid nodal voltages and MV-connected loads/generating units. The connected downstream LV systems also solve an OPF that accounts for the uncertainty of both nodal voltages imposed at the MV/LV interfaces and the LV-connected loads/generating units. Other MV-connected-controllable-distributed-resources also solve local optimization problems maximizing various utility functions while accounting for local constraints (e.g. a BESS ensuring its capacity constraints while maximizing usage profit). The aggregator and the local subproblems are derived and solved using the ADMM decomposition [26]. In short, the framework is formulated as a distributed optimization scheme where participating resources do not share their models. It therefore enables a distributed computation of the day-ahead dispatch plan accounting for the flexibility provided by several downstream networks and MV-connected-controllable-resources (e.g. BESS and PV units) without the explicit knowledge of their network or resource models, respectively. Additionally, to address the shortcomings of the works in the literature, grid-constraints are included in both the main aggregator and LV-subproblem OPFs by leveraging sensitivity coefficients-based linearizations of the power-flow equation. As a result, grid-losses are accounted for and linear constraints on nodal voltage and branch current magnitudes are included, in all the proposed OPFs. Finally, the proposed problem is validated through simulations performed on a MV system connected with two LV systems, one MW-scale battery, and several PV generation units.

Compared to existing literature, the main contribution of this work is the formulation of an algorithm that aggregates the available flexibilities (in terms of both power and energy) from downstream distribution networks without sharing their (sensitive) models while satisfying their internal constraints. The aggregated flexibility can participate to the day-ahead imbalance electricity market. Compared to [12,13,15], this work accounts for the operational constraints of the grid and proposes a convex problem. Furthermore, compared to [27], this work solves the problem in a distributed way, so explicit knowledge of the models of the participating resources is not required. Compared to [16], the grid constraints are better modeled by first-order Taylor's approximation.

The paper is organized as follows. Section 2 defines the problem statement, Section 3 presents the multi-grid dispatch formulation and its decomposition into distributed problems. Section 4 presents the test cases and results, and finally, Section 5 concludes the work.

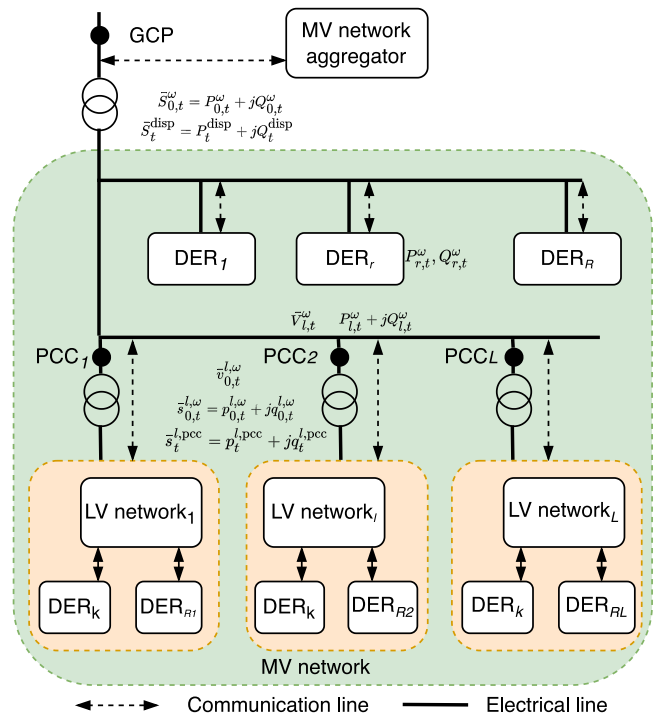

Fig. 1. Schematic showing the MV network architecture connected with multiple controllable and stochastic resources and downstream low voltage networks. The solid and dotted lines represent electrical and communication connections, respectively. The symbols are defined in Section 3.

2. Problem statement

Let us consider a MV distribution grid interfaced with multiple stochastic and controllable resources which can be controlled in real-time (e.g., PVs or BESSs). The MV grid is also interfaced with downstream LV distribution grids through MV/LV transformers. The LV systems also host stochastic resources such as PV plants and flexible resources such as BESSs. Fig. 1 shows the scheme of the considered power-system setup where the solid and dotted lines represent electrical and communication connections, respectively. The main objective of the proposed framework is to compute an optimal day-ahead dispatch at the grid connection point (GCP) of the MV grid. The day-ahead dispatch plan should account for

- the stochasticity of the electricity demand and generation in both MV and the LV networks;
- the flexibility and capability limits of the controllable resources in both MV and the LV networks;
- the operational constraints of MV and LV grids i.e. nodal voltage magnitudes within bounds, branch ampacities;

In this setup, we assume that parameters of the LV networks and the MV-connected-controllable-resources (MVCCRs) willing to participate in the dispatching, are not known to the MV aggregator. However, the former can share relevant information for the GCP dispatch plan to be optimally computed. More specifically, each LV system shares the power-flows and nodal voltage magnitudes at its point of common coupling (PCC) (see Fig. 1), and each MVCCR shares the apparent power flexibility they can offer within their capabilities.

In[1] all OPFs of this work, the grid operational constraints are modeled using sensitivity coefficient-based linearized power flow model

[1] In this work vectors and matrices are denoted by bold symbols. Complex number are denoted with a bar (e.g. $\bar{z} = |\bar{z}|\exp(j\theta)$) while their complex conjugates are underlined (e.g. $\underline{z}$).

(e.g. [28]). Let[2] N_b be the number of non-slack buses in the considered MV grid, N_l the number of lines, $\bar{\mathbf{V}} \in \mathbb{C}^{N_b}$ the nodal voltages, $\bar{\mathbf{I}} \in \mathbb{C}^{N_l}$ the branch currents, $\mathbf{P}, \mathbf{Q} \in \mathbb{R}$ the vectors containing controllable active and reactive injections, $P_d, Q_d \in \mathbb{R}$ the active and reactive aggregate grid losses; the grid model can be expressed for time t as

$$|\bar{\mathbf{V}}_t| = \mathbf{A}_t^v \begin{bmatrix} \mathbf{P}_t \\ \mathbf{Q}_t \end{bmatrix} + \mathbf{b}_t^v \tag{1}$$

$$|\bar{\mathbf{I}}_t| = \mathbf{A}_t^i \begin{bmatrix} \mathbf{P}_t \\ \mathbf{Q}_t \end{bmatrix} + \mathbf{b}_t^i \tag{2}$$

$$\begin{bmatrix} P_{d,t} \\ Q_{d,t} \end{bmatrix} = \mathbf{A}_t^d \begin{bmatrix} \mathbf{P}_t \\ \mathbf{Q}_t \end{bmatrix} + \mathbf{b}_t^d, \tag{3}$$

where $\mathbf{P}_t \in \mathbb{R}^{N_b}$ and $\mathbf{Q}_t \in \mathbb{R}^{N_b}$ are, respectively, nodal active and reactive power injections, $\mathbf{A}_t^v \in \mathbb{R}^{N_b \times 2N_b}$, $\mathbf{A}_t^i \in \mathbb{R}^{N_l \times 2N_b}$, $\mathbf{A}_t^d \in \mathbb{R}^{2 \times 2N_b}$, $\mathbf{b}_t^v \in \mathbb{R}^{N_b}$, $\mathbf{b}_t^i \in \mathbb{R}^{N_l}$, and $\mathbf{b}_t^d \in \mathbb{R}^2$ are state-dependent parameters enabling power-flow-linearizations, composed of constants and sensitivity coefficients (SCs) for time index t. SCs are formally defined as the partial derivative of controllable electric quantities (e.g. branch currents) w.r.t. control variables (i.e. nodal power injections). They are determined with the method in [28] by solving a system of linear equations (that admits a single solution, as proven in [29]) as a function of the grid's admittance matrix and the system state (i.e. nodal voltages at all buses). In the day-ahead phase, the SCs along the whole scheduling horizon are pre-computed using point predictions of the nodal injections. In the real-time phase, the SCs are updated at each control step using the present grid state. In the following, the linearization parameters for MV and lth LV systems for time t are denoted by $\mathbf{A}_t^{\mathrm{mv},v}, \mathbf{A}_t^{\mathrm{mv},i}, \mathbf{A}_t^{\mathrm{mv},d}, \mathbf{b}_t^{\mathrm{mv},v}, \mathbf{b}_t^{\mathrm{mv},i}, \mathbf{b}_t^{\mathrm{mv},d}$ and $\mathbf{A}_t^{\mathrm{lv}_l,v}$, $\mathbf{A}_t^{\mathrm{lv}_l,i}$, $\mathbf{A}_t^{\mathrm{lv}_l,d}$, $\mathbf{b}_t^{\mathrm{lv}_l,v}, \mathbf{b}_t^{\mathrm{lv}_l,i}, \mathbf{b}_t^{\mathrm{lv}_l,d}$ respectively.

3. Multi-grid day-ahead dispatch problem

In[3] the following, we present the aggregated day-ahead dispatch problem – referred to as multi-grid day-ahead dispatch – for a multi-grid system, i.e. MV grid connected to several LV networks and MVCCRs. First, the centralized problem is presented, then, to guarantee privacy and mimic real-world intra-grid-operator-relationships, i.e. the non-availability of LV downstream grid and MVCCR models at the MV aggregator level, a decomposition, leveraging distributed optimization relying on the ADMM, of the centralized dispatch problem is presented.

3.1. Design requirements of the dispatch plan

The main objective is to compute a day-ahead dispatch plan, i.e. the active power trajectory, that the MV distribution network advertises to its upstream network and should follow at its GCP during the next day of operation. As previously mentioned, since downstream LV network uncertainties and flexibilities are accounted for in the latter problem, the day-ahead dispatch plans at the different PCCs of the downstream grids are byproducts of the problem resolution. The design requirements of the proposed dispatch plan are:

- Stochastic variations from distributed generation and demand should be compensated by the LV-networks and MVCCRs while respecting their operational constraints.;
- Voltage uncertainties at the MV-GCP and, as a result, at the different LV-PCCs should be accounted for;
- The regulation made by MVCCRs and the controllable resources in the LV-downstream-grids should not violate MV and LV grid operation constraints.

The dispatch plan is computed with a stochastic optimization framework, where the stochasticity of distributed generation and demand nodal power injections is captured through scenarios. As previously discussed, grid operational constraints are modeled with a linearized grid model. Operational constraints of the controllable resources are modeled accounting for the PQ-capability-sets of their power converters and, in case these resources are BESS, also by state-of-energy constraints.

3.2. Centralized problem formulation

Let $\mathcal{L} := l = 1, \dots, L$ and $\mathcal{R} := r = 1, \dots, R$ be the set of indices of LV grids and MVCCRs, respectively that are connected to MV network. Let $\mathcal{T} = [t_0, t_1 \dots, t_N]$ be the set of time indices of the scheduling horizon delimited by t_0 and t_N. We assume the set $\Omega = \Omega^{\mathrm{mv}} \cup \bigcup_{l=1}^{\mathcal{L}} \Omega^{\mathrm{lv}_l}$ collects the scenarios ω for stochastic nodal-power-injections of uncontrollable generation and demand units, where Ω^{mv} and Ω^{lv_l} are scenario sets for the MV and lth LV networks, respectively. $\mathbf{P}_t^\omega, \mathbf{Q}_t^\omega$ and $\mathbf{P}_{t,\mathrm{unc}}^\omega, \mathbf{Q}_{t,\mathrm{unc}}^\omega$ contain controllable, i.e. aggregate LV-PCC and MVCCRs, and uncontrollable nodal active/reactive power injections of the MV system for timestep t and scenario ω. Similarly, $\mathbf{p}_t^{l,\omega}, \mathbf{q}_t^{l,\omega}$ and $\mathbf{p}_{t,\mathrm{unc}}^{l,\omega}, \mathbf{q}_{t,\mathrm{unc}}^{l,\omega}$ contain the nodal active/reactive controllable and uncontrollable power injections for the $l-$ LV system ($l \in \mathcal{L}$). Let $\bar{S}_{0,t}^\omega = P_{0,t}^\omega + jQ_{0,t}^\omega$ be the nodal-apparent-power-injections at the slack bus of the MV network (i.e. GCP), $\bar{s}_{0,t}^{l,\omega} = p_{0,t}^{l,\omega} + jq_{0,t}^{l,\omega} = P_{l,t}^\omega + jQ_{l,t}^\omega$ the nodal-apparent-power-injections at slack bus of lth LV network (lth PCC), $\bar{v}_{0,t}^{l,\omega} = \bar{V}_{l,t}^\omega$ the nodal voltage at the lth PCC, $\bar{S}_t^{\mathrm{disp}} = P_t^{\mathrm{disp}} + jQ_t^{\mathrm{disp}}$ the decision variable for the main MV-dispatch plan for time t, where P_t^{disp} and Q_t^{disp} refer to the active and reactive nodal powers, $\bar{s}_t^{l,\mathrm{pcc}} = p_t^{l,\mathrm{pcc}} + jq_t^{l,\mathrm{pcc}}$ the auxiliary decision variable for the lth LV network-dispatch plan at the lth PCC. The variables $P_{r,t}^\omega, Q_{r,t}^\omega$ denote the active and reactive nodal power injections of MVCCRs $r \in \mathcal{R}$. The lth LV network is also connected with controllable resources with indices defined by set $\mathcal{R}_l := r_l = 1, \dots, R_l$ with active and reactive nodal power injections (decision variables) denoted by $p_{r,t}^{l,\omega}, q_{r,t}^{l,\omega}$ for time t and scenario ω. The symbols $p_{d,t}^{l,\omega}, q_{d,t}^{l,\omega}$ denote aggregated active and reactive grid losses of lth LV network for time t and scenario ω.

The main idea behind the proposed formulation is to determine a main dispatch plan at the MV network GCP such that it can be tracked for any of the forecasted scenarios. The problem consists in determining the injections of the controllable resources (in both MV and LV grids) so as to minimize:

- The deviation between the MV dispatch plan $\bar{S}^{\mathrm{disp}}$ and its slack (i.e. GCP) nodal apparent power injections S_0^ω for all the scenarios $\omega \in \Omega$ and timesteps $t \in \mathcal{T}$;
- The deviation between the LV dispatch plan $\bar{s}^{l,\mathrm{pcc}}$ and its slack (i.e. lth PCC) nodal apparent power injections $\bar{s}_0^{l,\omega}$ for all the scenarios $\omega \in \Omega$, timesteps $t \in \mathcal{T}$ and all LV-grids $l \in \mathcal{L}$;
- MV-resource-specific costs $f_r(P_{r,t}, Q_{r,t})$ that reflect the willingness of each MVCCR to provide regulating power (specific cost functions can be found in Section 3.5);
- LV-controllable-resource-specific costs $f_r^l(p_{r,t}^l, q_{r,t}^l)$ that reflect their willingness to provide regulating power (specific cost functions can be found in Section 3.5)

The proposed centralized problem can therefore be written as[4]:

$$\begin{aligned} \hat{\bar{S}}^{\mathrm{disp}} = \underset{\bar{s}^{l,\mathrm{pcc}}, \bar{S}^{\mathrm{disp}},}{\arg\min} \sum_{\omega \in \Omega} \sum_{t \in \mathcal{T}} \Bigg\{ & \left\| \bar{S}_{0,t}^\omega - \bar{S}_t^{\mathrm{disp}} \right\|^2 + \sum_{r \in \mathcal{R}} f_r(P_{r,t}^\omega, Q_{r,t}^\omega) \\ & + \sum_{l \in \mathcal{L}} \left(\left\| \bar{s}_{0,t}^{l,\omega} - s_t^{l,\mathrm{pcc}} \right\|^2 + \sum_{r \in \mathcal{R}_l} f_r^l(p_{r,t}^{l,\omega}, q_{r,t}^{l,\omega}) \right) \Bigg\} \end{aligned} \tag{4}$$

subject to the following constraints.

[2] All non-slack nodes are modeled as PQ-injection nodes.

[3] In the following all electric quantities are expressed in per unit as we are dealing with multi-voltage-layer grids.

[4] The symbol $\|.\|$ refers to norm-2.

3.2.1. Constraints of the MV system

The linearized power flow at the GCP and grid losses equality constraints. The linearizations w.r.t. nodal power injections are given by (5a)–(5c).

$$P^{\omega}_{0,t} = \sum_{r\in\mathcal{R}} P^{\omega}_{r,t} + \sum_{l\in\mathcal{L}} P^{\omega}_{l,t} + \mathbf{1}^T \mathbf{P}^{\omega}_{t,\text{unc}} + P^{\omega}_{d,t} \;\; \forall t\in\mathcal{T}, \omega\in\Omega, \tag{5a}$$

$$Q^{\omega}_{0,t} = \sum_{r\in\mathcal{R}} Q^{\omega}_{r,t} + \sum_{l\in\mathcal{L}} Q^{\omega}_{l,t} + \mathbf{1}^T \mathbf{Q}^{\omega}_{t,\text{unc}} + Q^{\omega}_{d,t} \;\; \forall t\in\mathcal{T}, \omega\in\Omega, \tag{5b}$$

$$\begin{bmatrix} P^{\omega}_{d,t} \\ Q^{\omega}_{d,t} \end{bmatrix} = \mathbf{A}^{\text{mv},d}_{t,\omega} \begin{bmatrix} \mathbf{P}^{\omega}_{t} \\ \mathbf{Q}^{\omega}_{t} \end{bmatrix} + \mathbf{b}^{\text{mv},d}_{t,\omega} \;\; \forall t\in\mathcal{T}, \omega\in\Omega, \tag{5c}$$

The minimum power factor constraint[5] at the GCP imposed by a $\cos(\theta)_{\min}$

$$|P^{\omega}_{0,t}|/|\bar{S}^{\omega}_{0,t}| \geq \cos(\theta)_{\min} \qquad \forall t\in\mathcal{T}, \omega\in\Omega, \tag{5d}$$

The limits on the nodal voltages by bound magnitudes $[V^{\min}, V^{\max}]$ and currents $\mathbf{I}^{\max}$ by lines' ampacities)

$$V^{\min} \leq \mathbf{A}^{\text{mv},v}_{t,\omega} \begin{bmatrix} \mathbf{P}^{\omega}_{t} \\ \mathbf{Q}^{\omega}_{t} \end{bmatrix} + \mathbf{b}^{\text{mv},v}_{t,\omega} \leq V^{\max} \;\; \forall t\in\mathcal{T}, \omega\in\Omega, \tag{5e}$$

$$0 \leq \mathbf{A}^{\text{mv},i}_{t,\omega} \begin{bmatrix} \mathbf{P}^{\omega}_{t} \\ \mathbf{Q}^{\omega}_{t} \end{bmatrix} + \mathbf{b}^{\text{mv},i}_{t,\omega} \leq \mathbf{I}^{\max} \quad \forall t\in\mathcal{T}, \omega\in\Omega. \tag{5f}$$

3.2.2. Constraints for MVCCRs

The PQ-capability-set limits denoted by.[6]

$$\Phi_r(P^{\omega}_{r,t}, Q^{\omega}_{r,t}) \leq 0 \;\; \forall t\in\mathcal{T}, \omega\in\Omega, r\in\mathcal{R}. \tag{6}$$

3.2.3. Constraints of the LV systems $\forall l\in\mathcal{L}$

The linearized power flows at the lth PCC and grid losses equality constraints. The linearizations w.r.t. nodal power injections are given by (7a)–(7c).

$$p^{l,\omega}_{0,t} = \sum_{r\in\mathcal{R}_l} p^{l,\omega}_{r,t} + \mathbf{1}^T \mathbf{p}^{l,\omega}_{t,\text{unc}} + p^{l,\omega}_{d,t} \;\; \forall t\in\mathcal{T}, \omega\in\Omega, \tag{7a}$$

$$q^{l,\omega}_{0,t} = \sum_{r\in\mathcal{R}_l} q^{l,\omega}_{r,t} + \mathbf{1}^T \mathbf{q}^{l,\omega}_{t,\text{unc}} + q^{l,\omega}_{d,t} \;\; \forall t\in\mathcal{T}, \omega\in\Omega, \tag{7b}$$

$$\begin{bmatrix} p^{l,\omega}_{d,t} \\ q^{l,\omega}_{d,t} \end{bmatrix} = \mathbf{A}^{\text{lv}_l,d}_{t,\omega} \begin{bmatrix} \mathbf{p}^{l,\omega}_{t} \\ \mathbf{q}^{l,\omega}_{t} \end{bmatrix} + \mathbf{b}^{\text{lv}_l,d}_{t,\omega} \;\; \forall t\in\mathcal{T}, \omega\in\Omega. \tag{7c}$$

The voltage imposed by the MV system at LV's PCC is

$$|\bar{V}^{\omega}_{l,t}| = |\bar{v}^{l,\omega}_{0,t}| \;\; \forall t\in\mathcal{T}, \omega\in\Omega, \tag{7d}$$

The minimum power factor constraint at the lth PCC imposed by $\cos(\theta)_{\min,l}$

$$|p^{l,\omega}_{0,t}|/|\bar{s}^{l,\omega}_{0,t}| \geq \cos(\theta)_{\min,l} \qquad \forall t\in\mathcal{T}, \omega\in\Omega. \tag{7e}$$

The nodal voltages magnitudes bounded by voltage limits $[v^{\min,l}, v^{\max,l}]$ and branch current magnitude constraints by its ampacities $\mathbf{i}^{\max}_l$ given by

$$v^{\min,l} \leq \mathbf{A}^{\text{lv}_l,v}_{t,\omega} \left[\mathbf{p}^{\omega}_t \;\; \mathbf{q}^{\omega}_t\right]^T + \mathbf{b}^{\text{lv}_l,l}_{t,\omega} \leq v^{\max,l} \;\; \forall t\in\mathcal{T}, \omega\in\Omega, \tag{7f}$$

$$0 \leq \mathbf{A}^{\text{lv}_l,i}_{t,\omega} \left[\mathbf{p}^{\omega}_t \;\; \mathbf{q}^{\omega}_t\right]^T + \mathbf{b}^{\text{lv}_l,i}_{t,\omega} \leq \mathbf{i}^{\max}_l \quad \forall t\in\mathcal{T}, \omega\in\Omega. \tag{7g}$$

The constraints of the controllable resources[7] connected to LV networks are denoted by

$$\Phi^l_r(p^{l,\omega}_{r,t}, q^{l,\omega}_{r,t}) \leq 0 \;\; \forall t\in\mathcal{T}, \omega\in\Omega, r\in\mathcal{R}_l. \tag{8}$$

Once the problem in (3.2) is solved, the dispatch plans are the real part of its solution $\hat{S}^{\text{disp}}, \hat{s}^{l,\text{pcc}}$:

$$\hat{P}^{\text{disp}} = \Re\left\{\hat{S}^{\text{disp}}\right\}, \qquad \hat{p}^{l,\text{pcc}} = \Re\left\{\hat{s}^{l,\text{pcc}}\right\} \qquad \forall l\in\mathcal{L}. \tag{9}$$

3.3. ADMM-based distributed decomposition

The problem formulation in Section 3.2 is centralized, thus, it requires to know the parameters and model of each of the connected LV network and resources. However, this is not practical in real-life. Also, it has poor scalability due to increased amount of decision variables. Using ADMM-based distributed optimization, this problem can be reformulated into individual local problems and one global problem which can be solve iteratively. The problem is a standard sharing problem and separable in original decision variables of the local problems. It can be solved in a distributed manner by each resources; then, the solutions from each local problem are sent to the aggregator that accounts for the global constraints and objectives. It is achieved by introducing set of auxiliary variables into the aggregator problem which mimic the solutions of the local subproblems. We introduce $\tilde{P}^{\omega}_{r,t}, \tilde{Q}^{\omega}_{r,t}$ that represent local variables for active and reactive powers from MVCCRs such that

$$P^{\omega}_{r,t} = \tilde{P}^{\omega}_{r,t} \qquad \forall l\in\mathcal{L}, t\in\mathcal{T}, \omega\in\Omega \tag{10a}$$

$$Q^{\omega}_{r,t} = \tilde{Q}^{\omega}_{r,t} \qquad \forall l\in\mathcal{L}, t\in\mathcal{T}, \omega\in\Omega. \tag{10b}$$

For the LV grids connected to the MV network, power flows and voltage magnitudes seen at the respective MV nodes should be duplicated to LV's PCCs. It is given by

$$P^{\omega}_{l,t} = p^{l,\omega}_{0,t} \qquad \forall l\in\mathcal{L}, t\in\mathcal{T}, \omega\in\Omega \tag{11a}$$

$$Q^{\omega}_{l,t} = q^{l,\omega}_{0,t} \qquad \forall l\in\mathcal{L}, t\in\mathcal{T}, \omega\in\Omega \tag{11b}$$

(7d) (11c)

We define augmented Lagrangian by using a sequence of Lagrangian multipliers $y^{p,\omega}_{l,t}$, $y^{q,\omega}_{l,t}$, $y^{v,\omega}_{l,t}$, $y^{p,\omega}_{r,t}$, $y^{q,\omega}_{r,t}$ for each of the coupling constraints in (10) and (11). It is

$$\begin{aligned} L_\rho = & \sum_{\omega\in\Omega}\sum_{t\in\mathcal{T}} \Bigg\{ \left\|\bar{S}^{\omega}_{0,t} - \bar{S}^{\text{disp}}_t\right\|^2 + \sum_{r\in\mathcal{R}} f_r(P^{\omega}_{r,t}, Q^{\omega}_{r,t}) \\ & + \sum_{l\in\mathcal{L}}\left(\left\|\bar{s}^{l,\omega}_{0,t} - s^{l,\text{pcc}}_t\right\|^2 + \sum_{r\in\mathcal{R}_l} f^l_r(p^{l,\omega}_{r,t}, q^{l,\omega}_{r,t})\right) + \\ & \frac{\rho}{2}\sum_{l\in\mathcal{L}}\left\{\left\|P^{\omega}_{l,t} - p^{l,\omega}_{0,t}\right\|^2 + \left\|Q^{\omega}_{l,t} - q^{l,\omega}_{0,t}\right\|^2 + \left\||\bar{V}^{\omega}_{l,t}| - |\bar{v}^{l,\omega}_{0,t}|\right\|^2\right\} + \\ & \frac{\rho}{2}\sum_{r\in\mathcal{R}}\left\{\left\|P^{\omega}_{r,t} - \tilde{P}^{\omega}_{r,t}\right\|^2_2 + \left\|Q^{\omega}_{r,t} - \tilde{Q}^{\omega}_{r,t}\right\|^2_2\right\} + \\ & \sum_{l\in\mathcal{L}}\left\{y^{p,\omega}_{l,t}(P^{\omega}_{l,t} - p^{l,\omega}_{0,t}) + y^{q,\omega}_{l,t}(Q^{\omega}_{l,t} - q^{\omega}_{0,t}) + y^{v,\omega}_{l,t}(|\bar{V}^{\omega}_{l,t}| - |\bar{v}^{l,\omega}_{0,t}|)\right\} \\ & \sum_{r\in\mathcal{R}}\left\{y^{p,\omega}_{r,t}(P^{\omega}_{r,t} - \tilde{P}^{\omega}_{r,t}) + y^{q,\omega}_{r,t}(Q^{\omega}_{r,t} - \tilde{Q}^{\omega}_{r,t})\right\}\Bigg\}. \end{aligned} \tag{12}$$

subject to, (5), (6), (7) and (8). Here, ρ refers to the penalty parameter. Let us define scaled dual variables $u = y/\rho$ for all the Langrange multipliers denoted by $u^{p,\omega}_{l,t}$, $u^{q,\omega}_{l,t}$, $u^{v,\omega}_{l,t}$, $u^{p,\omega}_{r,t}$, $u^{q,\omega}_{r,t}$. The above problem can be solved in following three iterative steps using the scaled-ADMM sharing problem [26]. The iterative steps are summarized in the Algorithm 1. Here, k refers to the iteration index of ADMM. Fig. 2 shows the information flow for the ADMM-based dispatch computation. First, the original variables in (13) are computed in parallel for each MVCCRs and downstream LV networks. The updates of the copied variables in (14), require collecting the local solutions, and it is solved by the MV aggregator. Also, the dual variables in (15) are sent to local subproblems by the aggregator. Then, the updated solutions of the copied and dual updated are disseminated to the resources. Eqs. (13), (14), and (15) are solved till convergence criteria is met, i.e., when the primal and dual residual norms [26] reduce below a tolerance limit. For the penalty parameter ρ, we follow a self-adaptive approach as described in [26,31].

[5] The constraints is non-convex and infeasible when the real power at the GCP is zero. We use the convexification approach proposed in [30]. They are briefly described in Appendix A.1.

[6] The resource objectives and constraints are detailed in Section 3.5.

[7] It is assumed that LV networks know the models of their controllable resources; thus, they are included within LV constraints. This is unlike MVCCRs, of which models are not known to the MV network.

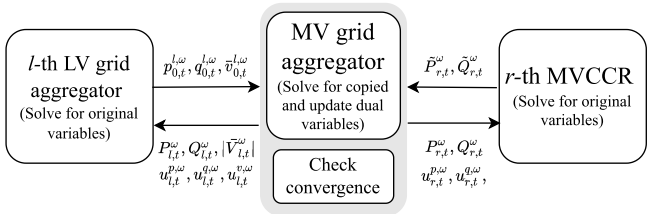

Fig. 2. Information exchange during the ADMM iterations.

3.4. Convergence criteria

The ADMM algorithm converges when the primal and dual residuals reduce below a feasibility tolerance bound. The primal residual is

$$s_{\text{pri}}(k+1) = \sum_{r\in\mathcal{R}}\sum_{\omega\in\Omega}\sum_{t\in\mathcal{T}}\left\|\begin{bmatrix}\tilde{P}_{r,t}^{\omega}(k+1)\\ \tilde{Q}_{r,t}^{\omega}(k+1)\end{bmatrix} - \begin{bmatrix}P_{r,t}^{\omega}(k+1)\\ Q_{r,t}^{\omega}(k+1)\end{bmatrix}\right\| + \sum_{l\in\mathcal{L}}\sum_{\omega\in\Omega}\sum_{t\in\mathcal{T}}\left\|\begin{bmatrix}p_{0,t}^{l,\omega}(k+1)\\ q_{0,t}^{l,\omega}(k+1)\\ |\bar{v}_{0,t}^{l,\omega}(k+1)|\end{bmatrix} - \begin{bmatrix}P_{l,t}^{\omega}(k+1)\\ Q_{l,t}^{\omega}(k+1)\\ |\bar{V}_{l,t}^{\omega}(k+1)|\end{bmatrix}\right\| \tag{16}$$

and the dual residual is

$$s_{\text{dual}}(k+1) = \sum_{r\in\mathcal{R}}\sum_{\omega\in\Omega}\sum_{t\in\mathcal{T}}\left\|\begin{bmatrix}P_{r,t}^{\omega}(k+1)\\ Q_{r,t}^{\omega}(k+1)\end{bmatrix} - \begin{bmatrix}P_{r,t}^{\omega}(k)\\ Q_{r,t}^{\omega}(k)\end{bmatrix}\right\| + \tag{17}$$

$$\sum_{l\in\mathcal{L}}\sum_{\omega\in\Omega}\sum_{t\in\mathcal{T}}\left\|\begin{bmatrix}P_{l,t}^{\omega}(k+1)\\ Q_{l,t}^{\omega}(k+1)\\ |\bar{V}_{l,t}^{\omega}(k+1)|\end{bmatrix} - \begin{bmatrix}P_{l,t}^{\omega}(k)\\ Q_{l,t}^{\omega}(k)\\ |\bar{V}_{l,t}^{\omega}(k)|\end{bmatrix}\right\|. \tag{18}$$

The convergence criteria is given by

$$s_{\text{pri}}(k+1) \le \epsilon_{\text{pri}}, \text{ and } s_{\text{dual}}(k+1) \le \epsilon_{\text{dual}} \tag{19}$$

where ϵ_{pri} and ϵ_{dual} are dynamic tolerance as defined in [26].

3.5. Example of controllable resource: the case of BESS

The objective is to compute power set-points while obeying physical limits on the power rating and reservoir size. We account for BESS losses by integrating its equivalent series resistance into the network admittance matrix using the method described in [30]. Let the series $P_{r,t}, Q_{r,t}$ be the decision variables for active and reactive power, the BESS decision problem is the following feasibility problem:

$$f_r(P_{r,t}, Q_{r,t}) = \sum_{t\in\mathcal{T}} 1 \tag{20a}$$

The set $\Phi_r(P_{r,t}, Q_{r,t})$ defines following set of constraints

$$\text{SOC}_t = \text{SOC}_{t-1} - P_{b,t}T_s/E_{\max}^b/3600 \qquad t\in\mathcal{T} \tag{20b}$$

$$0 \le (P_{b,t})^2 + (Q_{b,t})^2 \le (S_{\max}^b)^2 \qquad t\in\mathcal{T} \tag{20c}$$

$$a \le \text{SOE}_t \le (1-a) \qquad t\in\mathcal{T} \tag{20d}$$

where, SOC_t is the BESS state-of-charge, T_s is the sampling time (3600 s in this case), $S_{\max}^b$, and $E_{\max}^b$ are the power and reservoir capacities respectively, and $0 \le a < 0.5$ is a fixed parameter to specify a margin on SOE limits. The constraint (20c) is to restrict the battery's apparent power within its four-quadrant converter capability.

4. Simulation results and discussions

4.1. Multi-grid test case

We validate the proposed day-ahead dispatch computation for a multi-grid system shown in Fig. 3. It consists of two identical LV systems connected to nodes N_5 and N_6 of the MV network. The MV and LV networks are CIGRE benchmark test-cases [32] of nominal power/voltage ratings of 12 MVA/20 kV and 400 kVA/400 V respectively. The nominal demands and generation units are shown in Fig. 3. It also shows the capacity of the PV generation units and controllable resources. The capacity and the sites of the controllable and PV units are also summarized in Table 1.

Algorithm 1 ADMM

Require: $p_{0,t}^{l,\omega}(0), q_{0,t}^{l,\omega}(0), \bar{v}_{0,t}^{l,\omega}(0), \tilde{P}_{r,t}^{\omega}(0), \tilde{Q}_{r,t}^{\omega}(0), P_t^{l,\omega}(0), Q_t^{l,\omega}(0), |\bar{V}_t^{l,\omega}(0)|, P_{r,t}^{\omega}(0), Q_{r,t}^{\omega}(0), \rho > 0, k = 0$

while Convergence criteria (19) is not satisfied **do**

Solve local variables of lth LV networks $\forall\omega\in\Omega, t\in\mathcal{T}$

$$\begin{bmatrix}p_{0,t}^{l,\omega}(k+1)\\ q_{0,t}^{l,\omega}(k+1)\\ \bar{v}_{0,t}^{l,\omega}(k+1)\end{bmatrix} = \begin{cases}\underset{\substack{p_{0,t}^{l},q_{0,t}^{l}\\ s^{l,\text{pcc}}}}{\arg\min} \sum_{\omega\in\Omega}\sum_{t\in\mathcal{T}}\Big\{(s_{0,t}^{l,\omega} - s_t^{l,\text{pcc}})^2 + \\ \quad \sum_{r\in\mathcal{R}_l} f_r^l(p_{r,t}^{l,\omega}, q_{r,t}^{l,\omega}) + \\ \quad \frac{\rho}{2}\left\|P_{l,t}^{\omega}(k) - p_{0,t}^{l,\omega} + u_{l,t}^{p,\omega}(k)\right\|^2 + \\ \quad \frac{\rho}{2}\left\|Q_{l,t}^{\omega}(k) - q_{0,t}^{l,\omega} + u_{l,t}^{q,\omega}(k)\right\|^2 + \\ \quad \frac{\rho}{2}\left\||\bar{V}_{l,t}^{\omega}(k)| - |\bar{v}_{0,t}^{l,\omega}| + u_{l,t}^{v,\omega}(k)\right\|^2\Big\} \\ \text{subject to}: \ (7)\text{–}(8).\end{cases} \tag{13a}$$

and, solve local variables of rth MVCCRs, $\forall\omega\in\Omega, t\in\mathcal{T}$

$$\begin{bmatrix}\tilde{P}_{r,t}^{\omega}(k+1)\\ \tilde{Q}_{r,t}^{\omega}(k+1)\end{bmatrix} = \begin{cases}\underset{\tilde{P}_{r,t}^{\omega},\tilde{Q}_{r,t}^{\omega}}{\arg\min} \sum_{\omega\in\Omega}\sum_{t\in\mathcal{T}}\Big\{f_r(\tilde{P}_{r,t}^{\omega}, \tilde{Q}_{r,t}^{\omega}) + \\ \quad \frac{\rho}{2}\left\|P_{r,t}^{\omega}(k) - \tilde{P}_{r,t}^{\omega} + u_{r,t}^{p,\omega}(k)\right\|^2 + \\ \quad \frac{\rho}{2}\left\|Q_{r,t}^{\omega}(k) - \tilde{Q}_{r,t}^{\omega} + u_{r,t}^{q,\omega}(k)\right\|^2\Big\} \\ \text{subject to}: \ (6).\end{cases} \tag{13b}$$

Solve copied variables ($\forall\omega\in\Omega, t\in\mathcal{T}$)

$$\begin{bmatrix}P_{l,t}^{\omega}(k+1)\\ Q_{l,t}^{\omega}(k+1)\\ |\bar{V}_{l,t}^{\omega}(k+1)|\\ P_{r,t}^{\omega}(k+1)\\ Q_{r,t}^{\omega}(k+1)\end{bmatrix} = \begin{cases}\underset{\substack{S^{\text{disp}},P_{l,t},\\ Q_{l,t},|\bar{V}_{l,t}|}}{\arg\min} \sum_{\omega\in\Omega}\sum_{t\in\mathcal{T}}\Big\{(S_{0,t}^{\omega} - S_t^{\text{disp}})^2 + \\ \quad \sum_{l\in\mathcal{L}}\Big(\frac{\rho}{2}\left\|P_{l,t}^{\omega} - p_{0,t}^{l,\omega}(k) + u_{l,t}^{p,\omega}(k)\right\|^2 + \\ \quad \frac{\rho}{2}\left\|Q_{l,t}^{\omega} - q_{0,t}^{l,\omega}(k) + u_{l,t}^{q,\omega}(k)\right\|^2 + \\ \quad \frac{\rho}{2}\left\||\bar{V}_{l,t}^{\omega}| - |\bar{v}_{0,t}^{l,\omega}(k)| + u_{l,t}^{v,\omega}(k)\right\|^2\Big) + \\ \quad \sum_{r\in\mathcal{R}}\Big(\frac{\rho}{2}\left\|P_{r,t}^{\omega} - \tilde{P}_{r,t}^{\omega}(k) + u_{r,t}^{p,\omega}(k)\right\|^2 + \\ \quad \frac{\rho}{2}\left\|Q_{r,t}^{\omega} - \tilde{Q}_{r,t}^{\omega}(k) + u_{r,t}^{q,\omega}(k)\right\|^2\Big)\Big\} \\ \text{subject to}, (5).\end{cases} \tag{14}$$

Update dual variables ($\forall\omega\in\Omega, t\in\mathcal{T}$)

$$u_{l,t}^{p,\omega}(k+1) = u_{l,t}^{p,\omega}(k) + p_{0,t}^{l,\omega}(k+1) - P_{l,t}^{\omega}(k+1) \ \forall l\in\mathcal{L} \tag{15a}$$

$$u_{l,t}^{q,\omega}(k+1) = u_{l,t}^{q,\omega}(k) + q_{0,t}^{l,\omega}(k+1) - Q_{l,t}^{\omega}(k+1) \ \forall l\in\mathcal{L} \tag{15b}$$

$$u_{l,t}^{v,\omega}(k+1) = u_{l,t}^{v,\omega}(k) + |\bar{v}_{0,t}^{l,\omega}(k+1)| - |\bar{V}_{l,t}^{\omega}(k+1)| \ \forall l\in\mathcal{L} \tag{15c}$$

$$u_{r,t}^{p,\omega}(k+1) = u_{r,t}^{p,\omega}(k) + \tilde{P}_{r,t}^{\omega}(k+1) - P_{r,t}^{\omega}(k+1) \ \forall r\in\mathcal{R} \tag{15d}$$

$$u_{r,t}^{q,\omega}(k+1) = u_{r,t}^{q,\omega}(k) + \tilde{Q}_{r,t}^{\omega}(k+1) - Q_{r,t}^{\omega}(k+1) \ \forall r\in\mathcal{R} \tag{15e}$$

Check convergence (19).

$k \leftarrow k+1$

end while

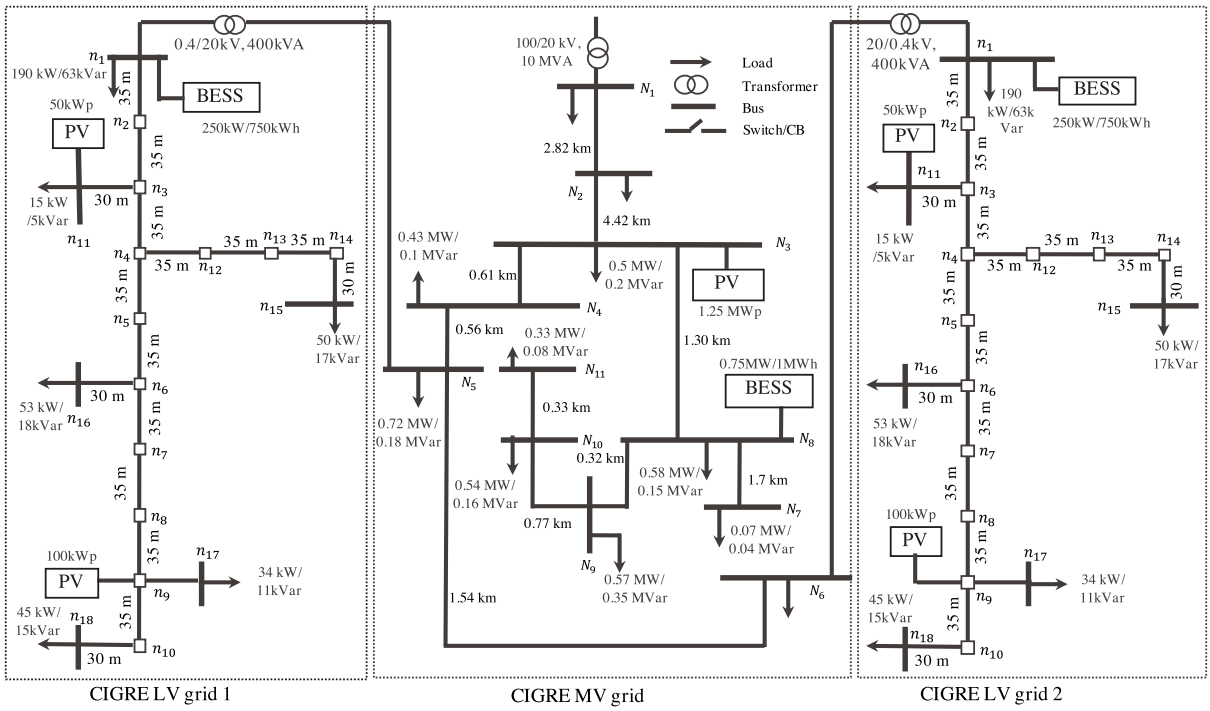

Fig. 3. Multi-grid test case: CIGRE MV and benchmark LV networks.

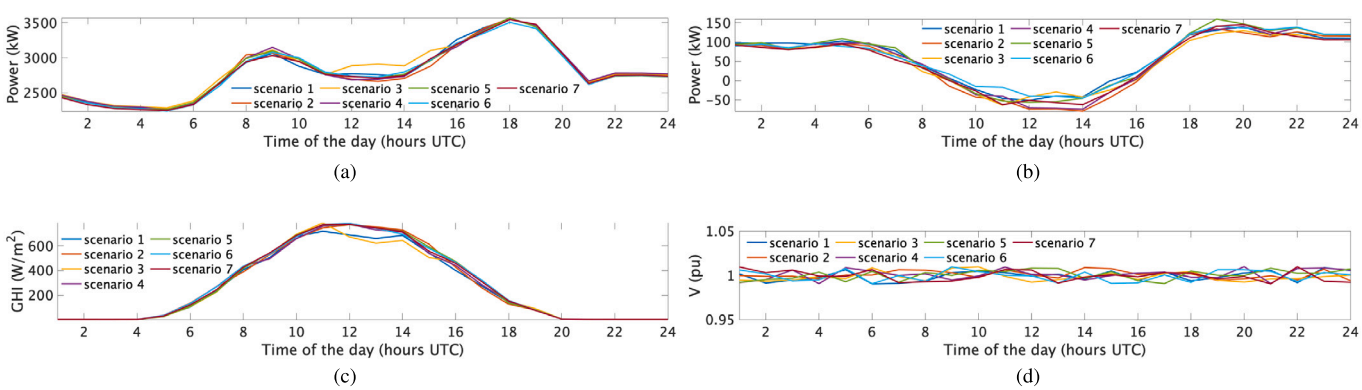

Fig. 4. Day-ahead scenarios of aggregated nodal active powers (in kW) for (a) MV network and (b) LV1 network, (c) GHI (in W/m^2) and (d) imposed voltage (in pu) at MV's GCP.

Table 1
Sites and sizes of BESS and PV units.

	PV		BESS	
	Node	Size	Node	Size
MV	N_3	1.25 [MWp]	N_8	0.75 [MW]/1.0 [MWh]
LV1	n_9 n_{11}	100 [kWp] 50 [kWp]	n_1	250 [kW]/750 [kWh]
LV2	n_9 n_{11}	100 [kWp] 50 [kWp]	n_1	250 [kW]/750 [kWh]

4.2. Day-ahead scenarios

Since the proposed framework is a scenario-based stochastic optimization, we forecast the uncertainties of the demand and generation by a set of scenarios that are forecasted in day-ahead. The scenarios (shown in Fig. Fig. 4) are modeled using the historical data, we use the scenario reduction and forecasting strategy from [24]. The scenarios are sampled at time-resolution $Ts = 3600$ s. For the load, it selects N_Ω scenarios[8] of 1-day time series of historical measurements of demand according to the day-type (working day, weekend, day of the week, the period of the year). The PV generation is forecasted starting from the predictions of the time-series of the global horizontal irradiance (GHI). We use GHI predictions scheme of [24]. We also model the uncertainty on the voltage imposed at the MV network's GCP from the upstream transmission system. This is done by obtaining the cumulative distribution function of the voltage variations using historical data from a real Swiss MV distribution network. As per the historical data, the voltage at the GCP was found to be varying uniformly within [0.98, 1.02] pu, so we generated the scenarios by a uniform distribution. Figs. 4(a) and 4(b) show the scenarios for aggregated prosumption at MV's GCP and LV1's PCC respectively. Fig. 4(c) shows the scenarios for

[8] The selection of ideal N_Ω is beyond the scope of this work, we determine $N_\Omega = 7$ that covers 95 percentile of the variation during the realization.

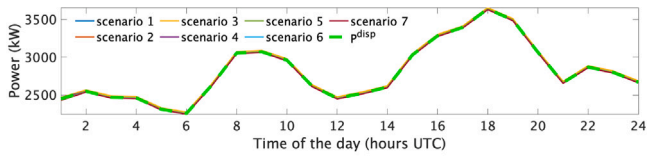

(a) Computed dispatch plan and aggregated active power at the MV's GCP.

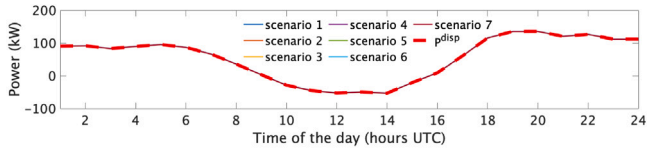

(b) Computed dispatch plan and aggregated active power at the LV1's GCP.

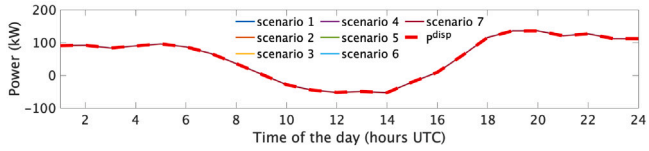

(c) Computed dispatch plan and aggregated active power at the LV2's GCP.

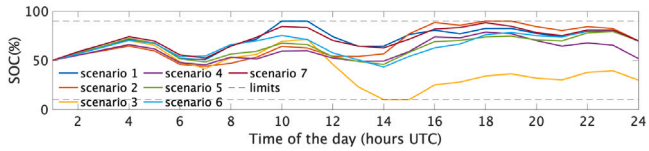

(d) SOC of MV's BESS for different scenarios.

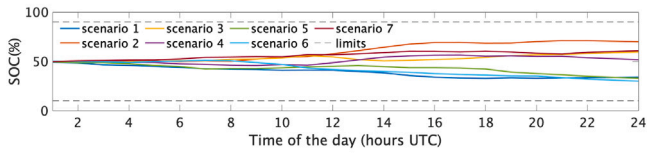

(e) SOC of LV1's BESS for different scenarios.

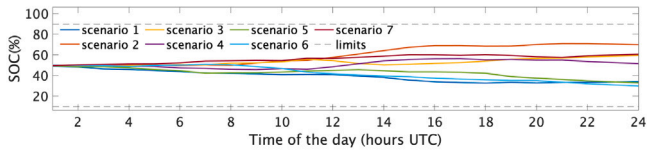

(f) SOC of LV2's BESS for different scenarios.

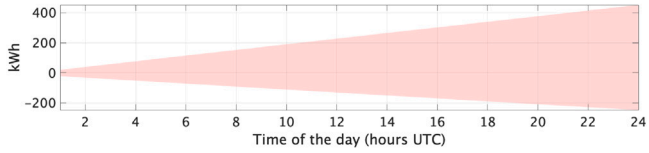

(g) Uncovered energy error for the dispatch plan at MV GCP.

Fig. 5. Dispatch plan computation for no-coordination case among MV and LV networks.

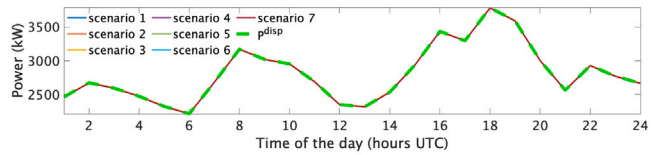

(a) Computed dispatch plan and aggregated active power at the MV's GCP.

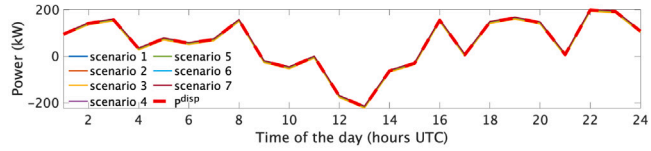

(b) Computed dispatch plan and aggregated active power at the LV1's GCP.

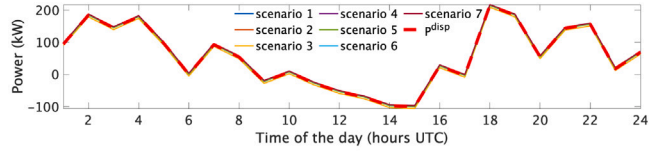

(c) Computed dispatch plan and aggregated active power at the LV2's GCP.

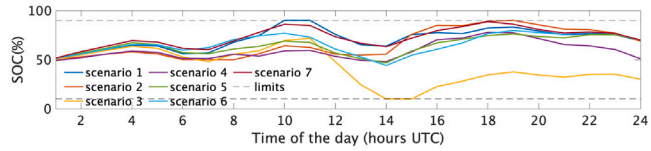

(d) SOC of MV's BESS for different scenarios.

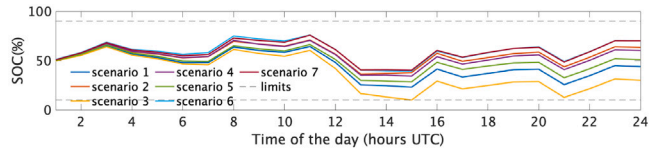

(e) SOC of LV1's BESS for different scenarios.

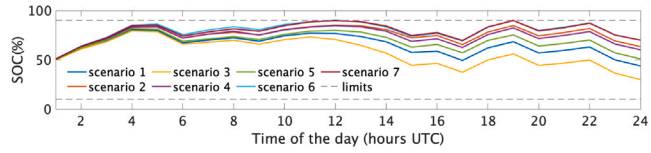

(f) SOC of LV2's BESS for different scenarios.

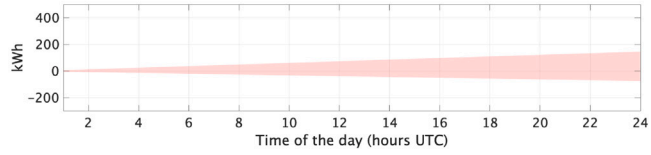

(g) Uncovered energy error for the dispatch plan at MV GCP.

Fig. 6. Dispatch plan computation for ADMM-based coordination of the MV and LV networks.

GHI, they are same for both LV and MV systems. Fig. 4(d) shows the profile for MV's GCP voltage in per units.

4.3. Simulation results

Using the day-ahead forecast scenarios of the load, generation and MV GCP voltage, we compute the day-ahead dispatch plan for the multi-grid system of Fig. 3. We show the computed dispatch plan at the MV's GCP and the PCCs of both LV networks. We also show the SOC of the BESS installed in both MV and LV systems. We simulate two cases:

- *No-coordination:* we define a base case where the MV system does not account for the flexibility of downstream LV networks. In this case, MV and LV networks operate as standalone systems, i.e. LV networks compute their dispatch plan and send it to the MV network. Then, MV system computes its dispatch plan by modeling LV networks as uncontrollable load.
- *Multi-grid dispatch using ADMM-based coordination:* we solve the proposed distributed dispatch computation of Algorithm 1. As developed in Section 3.3, this scheme coordinates with the downstream LV networks while computing the dispatch plans.

Table 2
Dispatch performance with and without coordination.

	MAE (kW)	UEE$^+$ (kWh)	UEE$^+$ (kWh)
No coordination	22	451	−247
Coordinated dispatch	6.5	146	−75

To quantify the difference in the tracking performance, Table 2 shows the performance comparison of two cases in terms of following metrics. The metrics are maximum absolute error (MAE),

$$\text{MAE} = \max_{\omega\in\Omega, t\in\mathcal{T}} |P_t^{\text{disp}} - P_{0,t}^{\omega}| \tag{21}$$

and uncovered energy error (UEE) defined as follows.

$$\text{UEE}^+ = \frac{T_s}{3600}\sum_{t\in\mathcal{T}}(\max_{\omega\in\Omega} P_{0,t}^{\omega} - P_t^{\text{disp}}) \tag{22}$$

$$\text{UEE}^- = \frac{T_s}{3600}\sum_{t\in\mathcal{T}}(\min_{\omega\in\Omega} P_{0,t}^{\omega} - P_t^{\text{disp}}) \tag{23}$$

4.3.1. No-coordination among MV and LV systems

Fig. 5 presents the simulation results for the no-coordination case. Figs. 5(a), 5(b), and 5(c) show the computed dispatch plans and the compressed scenarios (in different line-color plots) of the power at the GCP/PCC for MV, LV1, and LV2 networks, respectively. Figs. 5(d), 5(e) and 5(f) show the SOC plots for BESSs connected to MV, LV1, and LV2 networks and for different day-ahead scenarios. Finally, the uncovered energy error (i.e., the cumulative difference between the maximum/minimum day-ahead scenario and the dispatch plan) is shown in Fig. 5(g). Table 2 reports the tracking performance in terms of MAE and UEE$^+$/UEE$^-$.

As seen from the plot in Fig. 5(g) and metrics in Table 2, it can be concluded that the computed dispatch plan at the MV system produces UEE$^+$ and UEE$^-$ of 451 kWh and −247 kWh, respectively. It also has an MAE of 22 kW. In the no-coordination case, the BESS is the MV network's only controllable resource and reaches its state-of-charge bounds. For the LV systems, dispatch plans are well tracked, thanks to the compensation provided by their BESSs. From the SOC plots in Figs. 5(e) and 5(f), it can be noted that the BESS of LV networks are underutilized as their SOCs are always far from the saturation bounds.

4.3.2. Multi-grid dispatch using ADMM-based coordination among MV and LV systems

Fig. 6 shows the computed dispatch plan when the ADMM-based coordination is used. In this case, the BESSs from LV1 and LV2 networks compensate for the MV's dispatch plan error. From the uncovered energy plot in Fig. 6(g), and the metrics reported in Table 2, it can be concluded that the uncovered positive and negative energies at the MV system are reduced from 451 kWh and −247 kWh (in the no-coordination case) to 146 kWh and −75 kWh. Also, the MAE is reduced from 22 kW to 6.5 kW.

From the SOC plots of Figs. 6(e) and 6(f), it can be observed that LV's BESS are providing flexibility to the MV network. Also, the dispatch plans of the LV systems are different compared to the no-coordination case (Figs. 5(b)–5(c)) as LV networks provide flexibility to the upstream MV network to track its dispatch with high fidelity.

4.4. Further analysis

4.4.1. Case study with reduced line ampacity

To show the effectiveness of the coordination algorithm, we introduce congestion in the MV network by artificially reducing the ampacity of the line between nodes N_3 and N_8 by a factor of four. This binding constraint limits the power compensation provided by the MV BESS connected at node N_8. Again, we compare the coordinated vs. non-coordinated cases.

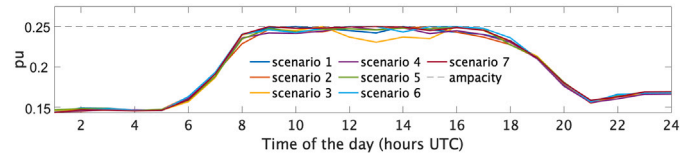

Fig. 7. Current in the line with reduced amapacity connecting nodes N_3 and N_8.

Table 3
Dispatch performance with and without coordination (Reduced ampacity in line connecting nodes N_3 and N_8.).

	MAE (kW)	UEE$^+$ (kWh)	UEE$^+$ (kWh)
No coordination	26	482	−270
Coordinated dispatch	8.2	161	−82

Table 4
Centralized vs. Distributed.

	TDE (MWh)	MinDP (MW)	MaxDP (kW)
Centralized	67.47	2.29	3.61
Distributed	67.36	2.29	3.55

Table 3 summarizes the metrics obtained for the two cases. Fig. 7 shows the line current flowing from node N_3 to N_8. As can be seen, the line current is reaching the ampacity limit from 8.00 to 18.00 h due to the power-flows caused by compensation provided by the MV's BESS. However, it always satisfies its ampacity limits, thanks to the OPF constraints. The compensation provided by BESSs of LV networks helps reducing the MAE and UEE in the coordinated case from 26 kW and 482 kWh/−270 kWh to 8.2 kW and 161 kWh/−82 kWh, respectively, as in the no-coordination case. It can be noted, the metrics of Table 3 are worse than the metrics presented in Table 2 due to the imposed reduced ampacity in the line connecting nodes N_3 and N_8.

4.4.2. Centralized vs. distributed

We compare the dispatch plan obtained by the ADMM-based coordination scheme with its centralized counterpart (Section 3.2). The comparison is shown in terms of total dispatched energy (TDE),

$$\text{TDE} = \frac{T_s}{3600}\sum_t P_t^{\text{disp}}, \tag{24}$$

maximum and minimum dispatched power,

$$\text{MaxDP} = \max_t P_t^{\text{disp}} \tag{25}$$

$$\text{MinDP} = \min_t P_t^{\text{disp}}. \tag{26}$$

These metrics for the dispatch plan of the MV system computed using distributed and centralized approaches are reported in Table 4. As observed, the dispatch plans computed using both approaches differ by 110 kWh in TDE and 60 kW in MaxDP. The difference is caused by tolerance bound (see convergence criteria in (19)) used for the convergence of ADMM-based distributed scheme. Thus, it can be concluded that the ADMM-based method converges to the solution (subject to the tolerance bound) of the original centralized problem of Section 3.2.

5. Conclusion

This work developed a framework to compute aggregated day-ahead dispatch plans of multiple and interconnected distribution grids operating at different voltage levels. It is achieved by accounting for the flexibility as well as the uncertainty of the downstream networks. The problem was formulated to determine the day-ahead dispatch plan of an MV network accounting for the flexibility offered by the downstream LV networks and from other MV-connected controllable resources. The problem was formulated as scenario-based stochastic

optimization where the day-ahead forecasts provide the uncertain load and generation scenarios. The optimization problem was solved by an ADMM-based distributed optimizations scheme guaranteeing better scalability and inter-grid-layer privacy.

The proposed framework was validated by simulating the CIGRE MV network connected with two identical CIGRE LV systems, controllable resources such as BESS, and stochastic resources such as PV generation units. The simulation concluded that the MV network manages to cover all the stochastic scenarios when downstream LV networks coordinate in providing flexibility to the MV network. In contrast, the MV aggregator failed to satisfy all the stochastic scenarios in no coordination case.

Future work would experimentally validate this framework on an actual interconnected distribution grid of the EPFL campus consisting of an MV network interfaced with an LV network.

CRediT authorship contribution statement

Rahul Gupta: Conceptualization, Methodology, Software, Validation, Visualization, Writing – original draft. **Sherif Fahmy:** Conceptualization, Methodology, Writing – review & editing. **Mario Paolone:** Supervision, Writing – review & editing, Resources, Project administration.

Declaration of competing interest

The authors declare that they have no known competing financial interests or personal relationships that could have appeared to influence the work reported in this paper.

Acknowledgments

This project is carried out within the frame of the research project "Pathways to an Efficient Future Energy System through Flexibility and Sector Coupling (PATHFNDR)" with the financial support of the Swiss Federal Office of Energy's "SWEET" program.

Appendix

A.1. Relaxation of the non-convex power factor constraint

We introduce two variables $P_{0,t}^{+,\omega}$ and $P_{0,t}^{-,\omega}$ such that

$$P_{0,t}^{\omega} = P_{0,t}^{+,\omega} - P_{0,t}^{-,\omega} \tag{27}$$

and replace Eq. (5d) with the following set of linear constraints:

$$P_{0,t}^{+,\omega} + P_{0,t}^{-,\omega} \geq Q_{0,t}^{\omega} \tan(\pi/2 - \theta_m) \tag{28}$$

$$P_{0,t}^{+,\omega} + P_{0,t}^{-,\omega} \geq -Q_{0,t}^{\omega} \tan(\pi/2 - \theta_m) \tag{29}$$

$$P_{0,t}^{+,\omega} \geq 0, P_{0,t}^{-,\omega} \geq 0, \tag{30}$$

where θ_m refers to the angle corresponding to $\cos(\theta)_{\min}$. The two terms of (27) $(p_{0,t}^{+,\omega}, p_{0,t}^{-,\omega})$ should be mutually exclusive. To this end, we augment the cost function (4) with the following new term

$$\sum_{\omega\in\Omega}\sum_{t\in\mathcal{T}} \nu\left((P_{0,t}^{+,\omega})^2 + (P_{0,t}^{-,\omega})^2\right) \tag{31}$$

that promotes $P_{0,t}^{+,\omega}, P_{0,t}^{-,\omega}$ being mutually exclusive, where $\upsilon \geq 0$ weighs the significance of obeying power factor constraints. Same procedure is used for LV systems.

References

[1] European Commission, Commission Regulation (EU) 2017/2195 of 23 November 2017 establishing a guideline on electricity balancing, Off. J. Eur. Union 312 (2017) 6–53.

[2] Swissgrid Ltd, Balancing Concept Switzerland: Industry Recommendation for the Swiss Power Market, Tech. Rep., Swissgrid Ltd, 2019.

[3] M. Braun, P. Strauss, A review on aggregation approaches of controllable distributed energy units in electrical power systems, Int. J. Distrib. Energy Res. 4 (4) (2008) 297–319.

[4] A. Losi, P. Mancarella, S. Mander, G. Valtorta, P. Linares, A. Horch, et al., Address Recommendations for Standard Committees, Regulators, Stakeholders Groups, Future R&D, Brussels, Belgium, 2013.

[5] Smart Grid Task Force, Regulatory Recommendations for the Deployment of Flexibility, EU SGTF-EG3 Report, 2015.

[6] M. Vallés, J. Reneses, R. Cossent, P. Frías, Regulatory and market barriers to the realization of demand response in electricity distribution networks: A European perspective, Electr. Power Syst. Res. 140 (2016) 689–698.

[7] M. Labatut, P. Mandatova, C. Renaud, Designing Fair and Equitable Market Rules for Demand Response Aggregation, EURELECTRIC, Tech. Rep., 2015.

[8] M. Kalantar-Neyestanaki, F. Sossan, M. Bozorg, R. Cherkaoui, Characterizing the reserve provision capability area of active distribution networks: A linear robust optimization method, IEEE Trans. Smart Grid 11 (3) (2019) 2464–2475.

[9] A.M. Carreiro, H.M. Jorge, C.H. Antunes, Energy management systems aggregators: A literature survey, Renew. Sustain. Energy Rev. 73 (2017) 1160–1172.

[10] A. La Bella, M. Farina, C. Sandroni, R. Scattolini, Design of aggregators for the day-ahead management of microgrids providing active and reactive power services, IEEE Trans. Control Syst. Technol. 28 (6) (2019) 2616–2624.

[11] O. Valarezo, T. Gómez, J.P. Chaves-Avila, L. Lind, M. Correa, D. Ulrich Ziegler, R. Escobar, Analysis of new flexibility market models in Europe, Energies 14 (12) (2021) 3521.

[12] A. Ouammi, H. Dagdougui, L. Dessaint, R. Sacile, Coordinated model predictive-based power flows control in a cooperative network of smart microgrids, IEEE Trans. Smart Grid 6 (5) (2015) 2233–2244.

[13] N. Nikmehr, S.N. Ravadanegh, Optimal power dispatch of multi-microgrids at future smart distribution grids, IEEE Trans. Smart Grid 6 (4) (2015) 1648–1657.

[14] D.A. Contreras, K. Rudion, Improved assessment of the flexibility range of distribution grids using linear optimization, in: 2018 Power Systems Computation Conference (PSCC), IEEE, 2018, pp. 1–7.

[15] M. Kahl, C. Freye, T. Leibfried, A cooperative multi-area optimization with renewable generation and storage devices, IEEE Trans. Power Syst. 30 (5) (2014) 2386–2395.

[16] P. Fortenbacher, et al., Grid-constrained optimal predictive power dispatch in large multi-level power systems with renewable energy sources, and storage devices, in: ISGT, Europe, IEEE, 2014, pp. 1–6.

[17] F. Sossan, E. Namor, R. Cherkaoui, M. Paolone, Achieving the dispatchability of distribution feeders through prosumers data driven forecasting and model predictive control of electrochemical storage, IEEE Trans. Sustain. Energy 7 (4) (2016) 1762–1777.

[18] C. Zhang, Y. Wang, Privacy-preserving decentralized optimization based on admm, 2017, arXiv preprint arXiv:1707.04338.

[19] R. Gupta, F. Sossan, E. Scolari, E. Namor, L. Fabietti, C. Jones, M. Paolone, An admm-based coordination and control strategy for pv and storage to dispatch stochastic prosumers: Theory and experimental validation, in: 2018 Power Systems Computation Conference (PSCC), IEEE, 2018, pp. 1–7.

[20] C. Zhang, M. Ahmad, Y. Wang, ADMM based privacy-preserving decentralized optimization, IEEE Trans. Inf. Forensics Secur. 14 (3) (2018) 565–580.

[21] X. Zhang, M.M. Khalili, M. Liu, Improving the privacy and accuracy of ADMM-based distributed algorithms, in: International Conference on Machine Learning, PMLR, 2018, pp. 5796–5805.

[22] T.W. Mak, F. Fioretto, P. Van Hentenryck, Privacy-preserving obfuscation for distributed power systems, Electr. Power Syst. Res. 189 (2020) 106718.

[23] X. Cao, J. Zhang, H.V. Poor, Z. Tian, Differentially private ADMM for regularized consensus optimization, IEEE Trans. Automat. Control 66 (8) (2020) 3718–3725.

[24] R.K. Gupta, F. Sossan, M. Paolone, Grid-aware distributed model predictive control of heterogeneous resources in a distribution network: Theory and experimental validation, IEEE Trans. Energy Convers. (2020).

[25] V. Dvorkin, F. Fioretto, P. Van Hentenryck, P. Pinson, J. Kazempour, Differentially private optimal power flow for distribution grids, IEEE Trans. Power Syst. 36 (3) (2020) 2186–2196.

[26] S. Boyd, N. Parikh, E. Chu, Distributed Optimization and Statistical Learning via the Alternating Direction Method of Multipliers, Now Publishers Inc, 2011.

[27] D. Contreras, O. Laribi, M. Banka, K. Rudion, Assessing the flexibility provision of microgrids in MV distribution grids, 2018.

[28] K. Christakou, J.-Y. LeBoudec, M. Paolone, D.-C. Tomozei, Efficient computation of sensitivity coefficients of node voltages and line currents in unbalanced radial electrical distribution networks, IEEE Trans. Smart Grid 4 (2) (2013) 741–750.

[29] M. Paolone, J.-Y. Le Boudec, K. Christakou, D.-C. Tomozei, Optimal Voltage Control Processes in Active Distribution Networks, Tech. Rep., The Institution of Engineering and Technology-IET, 2015.

[30] E. Stai, L. Reyes-Chamorro, F. Sossan, J.-Y. Le Boudec, M. Paolone, Dispatching stochastic heterogeneous resources accounting for grid and battery losses, IEEE Trans. Smart Grid 9 (6) (2017) 6522–6539.

[31] B. He, H. Yang, S. Wang, Alternating direction method with self-adaptive penalty parameters for monotone variational inequalities, J. Optim. Theory Appl. 106 (2) (2000) 337–356.

[32] CIGRE' Task Force C6.04.02, Benchmark Systems for Network Integration of renewable and Distributed Energy Resources, Tech. Rep., Cigre' International Council on large electric systems, 2009.